Int. J. Multiphase Flow Vol. 13, No. 4, pp. 511–533, 1987
Printed in Great Britain.

0301-9322/87 $3.00 + 0.00

TRAJECTORIES AND SINGULAR POINTS IN STEADY-STATE MODELS OF TWO-PHASE FLOWS

Z. BILICKI,† C. DAFERMOS, J. KESTIN, G. MAJDA‡ and D. L. ZENG§
Division of Engineering, Brown University, Providence, RI 02912, U.S.A.

(*Received* 7 *August* 1986; *in revised form* 1 *February* 1987)

Abstract—The purpose of this paper is to adapt the methodology of dynamical systems to the study of a wide class of mathematical models currently used to solve problems of steady 1-D two-phase flows. A detailed study of the geometrical features of the ensemble of solutions is then used for two purposes. First, it makes it possible to understand the physical characteristics of such flows without the need to produce complete solutions. Secondly, the methodology gives valuable indications as to how to supplement computer codes which become inadequate in the neighborhood of singular points. This leads to avoidable numerical difficulties and incorrect interpretations. This methodology is particularly useful in the study of the phenomena of cooking.

The important contribution of this general analysis is to show that, regardless of the number of equations in the model, the generic solutions involve only three types of singular points: saddle points, spirals or nodes.

By way of example, the method is applied to the mathematically simplest case, the homogeneous flow model with adiabatic boundary conditions. The channel consists of a convergent portion with transition to a divergent portion through a smooth throat. The divergent portion possesses an inflection point after which the rate of area divergence decreases. The fluid is a mixture of water and steam in thermodynamic equilibrium. The expected saddle point, located just downstream from the throat, is followed by an unexpected spiral. The phase space consisting of pressure P, enthalpy h and spatial coordinate z divides itself into four distinct areas. In area A of figure 13 all solutions are single-valued, possess a pressure minimum and correspond to physically acceptable subcritical flows. In area B the solutions of the differential equations (all possessing a turning point) are irrelevant for the physical problem at hand. Through the saddle point there passes a trajectory which is unique in the subcritical portion and continues with two branches, one subcritical ending at pressure P', the other supercritical, ending at pressure P''. Area C between those branches contains states which are not described by the postulated model. It is conjectured that flows against a back-pressure, $P'' < P_a < P'$, evidently observed in nature, must presumably be described by an extension to the model involving enhanced entropy production. The remaining area D contains supercritical state points and is of no present interest.

1. INTRODUCTION

The purpose of this paper is to assert that numerical solutions of problems in two-phase flows to be obtained with a computer code should be supplemented with a partially quantitative, but largely qualitative analysis of the topological patterns of solutions in phase space ("phase portraits") implied in the particular mathematical model employed. Since all 1-D mathematical models of steady two-phase flow now in use are of the form extensively explored for the analysis of dynamical systems, the engineer interested in solving problems in two-phase flow gains access to a wealth of useful mathematical results and techniques (e.g. Poincaré 1880, 1890, 1899; Hale 1969; Guckenheimer & Holmes 1983; Arnold 1973, 1978, 1982; Kaplan 1958; Kestin & Zaremba 1952, 1953, 1954; Bilicki & Kestin 1983; Perry 1984).

The method is geometric in nature, and our work demonstrates conclusively that the theory of singular points of systems of coupled, ordinary, nonlinear differential equations—still largely unexploited in this field—is essential for clarity, for the proper management of computer codes and for the understanding of the phenomenon of choking *as predicted by the adopted mathematical model*, an impossible task when only numerical procedures are used.

The kingpin of the analysis is the identification of the singular points of the basic system of equations and of the solution patterns that they imply. Such an analysis serves two purposes. First, it gives the analyst the ability to understand the physical characteristics of a class of flows without

†‡§Permanent addresses: †Institute of Fluid Flow Machinery, Polish Academy of Sciences, 80-952 Gdansk, Poland; ‡Department of Mathematics, Ohio State University, Columbus, OH 43210, U.S.A.; §Heat Power Engineering Department, Chongqing University, Chongqing, Sichuan, People's Republic of China.

the need to produce complete solutions. Secondly, it gives valuable indications as to how to supplement computer codes because practically all numerical methods of solution become inadequate in the neighborhood of the singular points and are constitutionally incapable of locating them in the first place, which leads to numerical difficulties and incorrect interpretations. This has to do with the fact that the set of algebraic equations, which the computer code must solve at each step, becomes either impossible or indeterminate (Delhaye *et al.* 1981; Bouré *et al.* 1976) and no longer solves the coupled differential equations of the model.

The plan of the paper is to identify the mathematical properties of a broad class of models of two-phase flows in three appendices and to devote the main text to the formulation of some general, physical conclusions supplemented by a detailed analysis of one very simple example. The example concerns flow through a convergent–divergent nozzle.

2. THE BASIC EQUATIONS

Practically all known mathematical models used for the analysis of steady-state 1-D two-phase flows of fluids can be brought to the form of the following ordinary differential vector equation:†

$$A_{ij}(\boldsymbol{\sigma})\frac{\mathrm{d}\sigma_i}{\mathrm{d}z} = b_j(\boldsymbol{\sigma}, z) \quad (i,j = 1, 2, \ldots, n). \tag{1}$$

Here $\boldsymbol{\sigma}(z)$ is a vector of n components of temporally- and spatially-averaged thermodynamic and dynamic quantities which is a function of a single independent variable z. Equation [1] represents a system of coupled, ordinary, nonlinear differential equations. This system, supplemented with the initial conditions

$$\sigma_i(0) = \sigma_{i\,0} \quad (i = 1, 2, \ldots, n), \tag{2}$$

constitutes an initial-value problem.

Since the analysis outlined here is topological in nature, the choice of the particular physical quantities as components of $\boldsymbol{\sigma}$ is secondary and can, therefore, be governed by practical considerations of convenience.

3. THE VELOCITY VECTOR IN THE PHASE SPACE

With very few exceptions, solutions of this problem must be obtained by the use of numerical methods and computer codes. Each solution represents a trajectory $\boldsymbol{\sigma}(z)$ in the phase space Ω of $n + 1$ dimensions which consists of the n components of $\boldsymbol{\sigma}$ and of coordinate z. The basic equation [1] defines a vector field $\mathbf{V}(\boldsymbol{\sigma}, z)$ in the phase space. Each vector of this field is tangential to the corresponding trajectory and its direction is specified by the n angles,

$$\alpha_i = \tan^{-1}\left(\frac{\mathrm{d}\sigma_i}{\mathrm{d}z}\right), \tag{3}$$

which it forms with the z-axis in the planes σ_i, z. We calculate the angles explicitly by application of Cramer's rule:

$$\frac{\mathrm{d}\sigma_i}{\mathrm{d}z} = \frac{N_i(\boldsymbol{\sigma}, z)}{\Delta(\boldsymbol{\sigma})} = A_{ij}^{-1} b_j. \tag{4}$$

Here

$$\Delta(\sigma) \triangleq \det(A_{ij}) \tag{5}$$

and the $N_i(\boldsymbol{\sigma}, z)$ are determinants, each obtained from A_{ij} by replacing the ith column by b_j. If we define the components of the vector $\mathbf{V}(\boldsymbol{\sigma}, z)$ as

$$\Delta, N_1 \ldots, N_n,$$

†Throughout the paper, use is made of the Einstein summation convection. When no subscripts are displayed, the corresponding boldface symbols denote vectors or tensors.

we notice that its directional angles $\alpha_1, \ldots, \alpha_n$ are those derived in [3]. Reference to the vector field $\mathbf{V}(\boldsymbol{\sigma}, z)$ proves to be convenient for numerical calculations and for the qualitative analysis which forms the gist of this paper.

4. THE AUTONOMOUS SYSTEM

At each point of the trajectory $\boldsymbol{\sigma}(z)$, the vector $\mathbf{V}$ can be interpreted as the velocity with which a point moves along the trajectory if a parameter t along it is arbitrarily defined. This leads us to the autonomous system

$$\begin{aligned} \frac{\mathrm{d}z}{\mathrm{d}t} &= \Delta(\boldsymbol{\sigma}) \\ \frac{\mathrm{d}\sigma_i}{\mathrm{d}t} &= N_i(\boldsymbol{\sigma}, z). \end{aligned} \qquad [6]$$

The components of this vector can be taken as Δ in the z-direction and N_i each in the direction of coordinate σ_i.

At points of the phase space for which $\Delta(\boldsymbol{\sigma}) = 0$ but not all N_i vanish, the vector $\mathbf{V}$ is normal to the z-axis. At points where $\Delta(\boldsymbol{\sigma}) = 0$ and all components $N_i(\boldsymbol{\sigma}, z)$ vanish, the direction of $\mathbf{V}$ is undefined since its magnitude is zero.

5. COMMON FEATURES OF ALL THE MATHEMATICAL MODELS

The majority of the 1-D models embodied in [1] regard the system as a single pseudo-fluid in which the two phases coexist at every point of the physical continuum or are present as two separated phases. The process is governed by the conservation laws which introduce the derivatives $\mathrm{d}\sigma_i/\mathrm{d}z$. Hence the components of the $n \times n$ matrix A_{ij} do not contain the space variable z. Depending on the model, the number of equations ranges from $n = 2$ upwards.

The conservation equations augmented by the equation of state must be supplemented by empirical closure conditions which define the covariances arising from averaging. In this paper we restrict attention to closure conditions which are given in terms of the components σ_i to the exclusion of their derivatives. These define the elements of vector b_j which now contains $\boldsymbol{\sigma}$ as well as z explicitly; its elements also depend on the given channel shape described by its area variation $A(z)$.

6. TOPOLOGICAL STRUCTURE OF THE PHASE SPACE

The phase space Ω is constructed of the $n + 1$ dimensions which enter [6], i.e. of z and the n components of $\boldsymbol{\sigma}$. In it, it is necessary to distinguish three classes of points: (a) regular points, (b) turning points and (c) singular points.

6.1. Regular points

A point $(z^\circ, \boldsymbol{\sigma}^\circ)$ in phase space is called *regular* if rank $[A_{ij}(\boldsymbol{\sigma}^\circ)] = n$ or, equivalently, if

$$\Delta(\boldsymbol{\sigma}) \neq 0. \qquad [7]$$

On the set of regular points the two systems, [1] and [4], are equivalent. Then the system satisfies the requirements of existence and uniqueness. If, and only if, all points along a trajectory satisfy [4], a numerical solution constitutes a proper approximation to an analytic solution. The initial-value problem has a unique solution in this case.

A unique *mathematical* solution to the system [1] does not necessarily represent a physically acceptable solution, as we shall point out where necessary. In this connection it must also be remembered that physically valid initial conditions [2] are prescribed at $z = 0$ and rule out all trajectories which do not reach the hyperplane $z = 0$.

6.2. The hypersurface $T(\Delta = 0)$

All points in phase space which satisfy the condition

$$\Delta(\sigma) = 0 \qquad [8]$$

are either turning points (z^*, σ^*) or singular points (z^{**}, σ^{**}). The set of points which satisfy this condition lie on a cylindrical hypersurface (*manifold* $\mathscr{T}$) of n dimensions whose generators are parallel to the z-axis. The properties of this manifold depend only on the terms of matrix A_{ij} and are thus independent of the closure conditions. At all points of $\mathscr{T}$ the rank of A_{ij} is at most $n-1$.

The hypersurface $\mathscr{T}$ has certain important properties which we now proceed to develop.

Condition [8] is an implicit equation in the components of σ, that is between the velocity or velocities (or, equivalently, specific flow rates) included in σ and the thermodynamic properties of the two phases. In all homogeneous flow models this condition is equivalent to the statement that the critical fluid velocity w^* is equal to the local speed of sound,

$$w^* = a = \left[\left(\frac{\partial P}{\partial \rho}\right)_s\right]^{\frac{1}{2}}. \qquad [9]$$

In the two-fluid model condition [8] states that the local (critical) barycentric velocity w_b^* is a weighted average of the speeds of sound, a_G and a_L in the two phases,

$$w_b^* = \frac{\left[(1-\alpha)\left(\frac{w_G}{w_L}\right)^2 \rho_G + \alpha\rho_L\right]\left[\alpha\rho_G + (1-\alpha)\rho_L\left(\frac{w_L}{w_G}\right)^2\right]}{\left[(1-\alpha)\frac{\rho_G}{a_L^2} + \frac{\alpha\rho_L}{a_G^2}\right][(1-\alpha)\rho_L + \alpha\rho_G]^2}. \qquad [10]$$

It follows that the cylindrical hypersurface $\mathscr{T}$ divides the phase space Ω into a region Ω_1 where $\Delta > 0$ and all local velocities are subscritical ($w < w^*$ or $w_b < w^*$), and into a supercritical region Ω_2 where $\Delta < 0$ ($w > w^*$ or $w_b > w^*$). This is suggested by the diagram in figure 1 which, of necessity, is drawn for $n = 2$.

In most practical problems, we are interested in flows which start at $z = 0$ with a relatively low, subcritical velocity (points in Ω_1) whose trajectories progress in the positive z-direction. Supercritical velocities at the inlet are not fundamentally excluded, but occur so rarely that we ignore them in this paper.

It will be shown in another place that the velocities w^* or w_b^* which satisfy [8] represent the speed of propagation of a plane wave of small amplitude because they correspond to a stationary characteristic of the (to be expected) hyperbolic partial differential equation which is a time-dependent extension of [1] (Bouré *et al.* 1976; Bouré 1977; Trapp & Ransom 1982). This feature links condition [8] with the occurrence of choking in the channel.

The preceding relations are independent of column vector b_j, i.e. of the closure conditions (source terms) and shape of the channel. In cases where body forces due to gravitation play a role, the above conclusions remain unaffected by them, because the gravitational acceleration appears only in b_j.

It is remarkable that in the presently discussed class of models the speed of propagation of a weak plane wave is insensitive to gravity, the shape of the channel and the nature of the source terms b_j in [1].

The distinction between turning points and singular points can be properly understood only in terms of a theorem of matrix algebra whose proof is given in Appendix A.

The condition $\Delta = 0$ defines the hypercylinder $\mathscr{T}$ and each of the n conditions $N_i = 0$ defines a hypersurface Σ_i. We center attention on the manifold $\mathscr{S}$ of $n-1$ dimensions which is the intersection of $\mathscr{T}$ with one hypersurface, say $\Sigma_1(N_1 = 0)$. We assume that the two hypersurfaces intersect transversely and state the criterion for this to be so in Appendix B. The theorem in question asserts that all $N_i = 0$ on $\mathscr{T}$, and this implies that all remaining hypersurfaces Σ_i must necessarily intersect $\mathscr{T}$ at $\mathscr{S}$.

This situation is illustrated with the aid of figure 2.

The points (z^*, σ^*) which belong to $\mathscr{T}$ but not to $\mathscr{S}$ are called *turning points*. The points (z^{**}, σ^{**}) which belong to $\mathscr{S}$ as well as to $\mathscr{T}$ are called *singular points*.

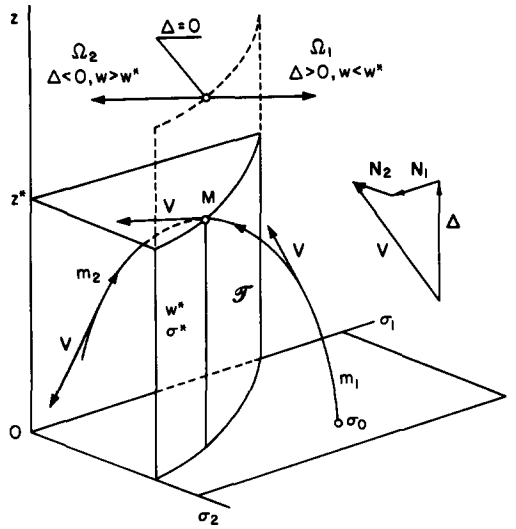

Figure 1. Phase space Ω and hypersurface $\mathscr{T}(\Delta = 0)$.

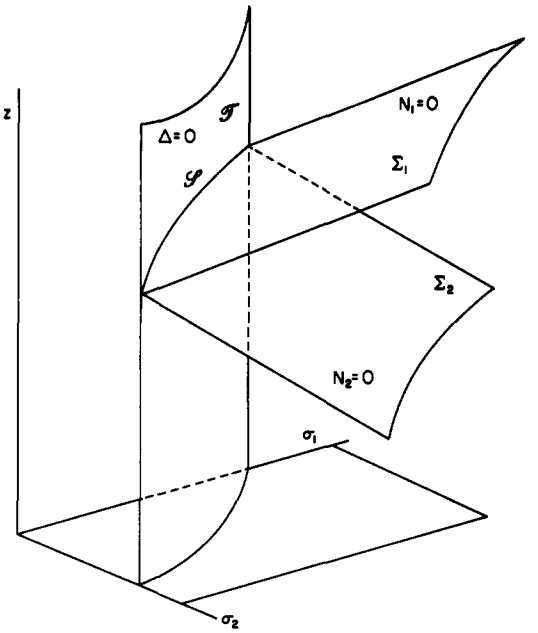

Figure 2. Definition of manifold $\mathscr{S}$ as the intersection between $\Delta = 0$ and all $N_i = 0$.

6.3. *Turning points*

A trajectory which passes through a turning point must have there a maximum or a minimum in z, or a point of inflection, because the vector V at such a point is normal to the z-axis and to the hypercylinder $\mathscr{T}$.

The diagram in figure 1 shows a trajectory m with a maximum at M on $\mathscr{T}$. Since the flow cannot change direction in the same channel, such a trajectory can be traversed only along the limb m_1 in the direction of V; all its points are then subcritical. The limb m_2, whose points are supercritical, also represents a possible solution when it is traversed in the direction opposite to V.

Clearly, state M cannot exist inside a channel but may occur at its end. Thus all trajectories whose maxima intersect $\mathscr{T}$ at $z < z^*$ must be ruled out as solutions of our physical problem for a channel of length $L = z^*$. All trajectories which pierce $\mathscr{T}$ at $z > z^*$ represent acceptable solutions for such a channel, and it is not difficult to show that the mass flow rate $\dot{m}$ is largest along trajectories with maximum at z^*, and we conclude that trajectories such as m_1 or m_2 represent choking at the end of the channel. Here $\Delta = 0$ is the "criterion of choking". Under such conditions, the channel exit blocks the upstream propagation of a pressure drop outside the channel, and its flow rate becomes independent of pressure decreases imposed outside the exit.

A trajectory which possesses a point of inflection on $\mathscr{T}$ (not shown) is not acceptable physically, because at such a point $|d\sigma/dz| \to \infty$, which is ruled out inside a channel, because the components of σ represent physical quantities, none of which can grow at an infinite rate. Similarly, a trajectory which has a minimum on $\mathscr{T}$ (not shown either) must also be ruled out as a physically valid solution because on either branch it would start with a large velocity, proceed in the negative z-direction and fail to reach $z = 0$.

6.4. *Nondegenerate singular points*

The singular points (z^{**}, σ^{**}) at which $\Delta = 0$ and all $N_i = 0$, for $i = 1, \ldots, n$, are precisely the equilibrium points (V = 0) of system [6]. A singular point is called *nondegenerate* if the rank of the matrix $A_{ij}(\sigma^{**})$, which is at most $n - 1$ on account of $\Delta(\sigma^{**}) = 0$, is precisely $n - 1$. Eschewing generality, we limit our discussion to nondegenerate singular points, because degenerate singular points represent nongeneric situations and are not likely to occur in practical flows. The set of nondegenerate singular points has been denoted by $\mathscr{S}$.

The importance of identifying the location and character of the singular points of [6], with an eye on numerical calculations, resides in the fact that they do not satisfy the uniqueness theorem.

The determination of the topological character of trajectories in the neighborhood of a singular point appears in its simplest form in the case of two linear ordinary differential equations with constant coefficients (e.g. Coddington & Levinson 1955; Kaplan 1958). The autonomous system

$$\frac{dx_1}{dt} = a_{11}x_1 + a_{12}x_2, \tag{11a}$$

$$\frac{dx_2}{dt} = a_{21}x_1 + a_{22}x_2, \tag{11b}$$

has a singular point at the origin $x_1 = x_2 = 0$ of the x_1, x_2 plane. Here

$$\sigma = \begin{bmatrix} x_1 \\ x_2 \end{bmatrix}, \quad a_{ij} = \begin{bmatrix} a_{11} a_{12} \\ a_{21} a_{22} \end{bmatrix}. \tag{12}$$

In this elementary example it is possible to write down the explicit solutions

$$x_1 = c_1 \xi_1 \exp(\lambda_1 t) + c_2 \eta_1 \exp(\lambda_2 t) \tag{13a}$$

and

$$x_2 = c_1 \xi_2 \exp(\lambda_1 t) + c_2 \eta_2 \exp(\lambda_2 t), \tag{13b}$$

where c_1 and c_2 are arbitrary constants. The exponential factors λ_1 and λ_2 are the two eigenvalues, here assumed distinct, of the matrix a_{ij}, so that

$$\begin{vmatrix} a_{11} - \lambda & a_{12} \\ a_{21} & a_{22} - \lambda \end{vmatrix} = 0. \tag{14}$$

The eigenvalues satisfy the explicit characteristic equation

$$\lambda^2 - (a_{11} + a_{22})\lambda + (a_{11}a_{22} - a_{21}a_{12}) = 0. \tag{15}$$

The vectors $\boldsymbol{\xi}(\xi_1, \xi_2)$ and $\boldsymbol{\eta}(\eta_1, \eta_2)$ are the eigenvectors which are implied in the equations

$$\lambda_1 \xi_i = A_{ij}\xi_j \quad (i, j = 1, 2) \tag{16a}$$

and

$$\lambda_2 \eta_i = A_{ij}\eta_{ij} \quad (i, j = 1, 2). \tag{16b}$$

The solutions quoted in (11a, b) admit three types of topological patterns—(a) saddle points, (b) nodes, (c) spirals (foci)—depending on the relationships obtaining between the constants; these are illustrated with the aid of figure 3 which correlates each pattern with the eigenvalues. In particular,

$$\left.\begin{aligned} &\text{(a) at saddle points,} \quad \lambda_1 < 0 < \lambda_2 \\ &\text{(b) at nodes,} \quad \lambda_1 < \lambda_2 < 0 \text{ or } \lambda_1 > \lambda_2 > 0 \\ &\text{(c) at spirals,} \quad \lambda_1 = \alpha + i\beta, \quad \lambda_2 = \alpha - i\beta, \quad \alpha, \beta \neq 0. \end{aligned}\right\} \tag{17}$$

We note for future reference that through

- a saddle point there pass exactly two trajectories
- a nodal point there passes an infinity of trajectories
- a spiral there pass no trajectories.

The principal question which arises in conjunction with the more complex system [6] of $n + 1$ nonlinear equations is to discover whether we must expect more complex patterns due to nonlinearity and more kinds of them as the number $n + 1$ increases beyond 2. The most important contribution of this paper is to demonstrate that this is *not* the case. Regardless of the number n

of equations in [1], it is possible to encounter *only* the above three kinds of *nondegenerate* singular points along any trajectory.†

More precisely, we shall state later, and prove in Appendices C and D, that the phase portrait in the vicinity of a nondegenerate singular point has the same topolgical structure as its linearized form. This result follows from an application of the "center manifold theorem", stated in Appendix D.

Since (z^{**}, σ^{**}) is an equilibrium point of [6], relevant information is provided by its linearized form about (z^{**}, σ^{**}) which reads

$$\frac{dX_\alpha}{dt} = e_{\alpha\beta} X_\beta, \qquad [18]$$

where $e_{\alpha\beta}(\alpha, \beta = 0, 1, \ldots, n)$ is the $(n+1) \times (n+1)$ Jacobian matrix given by

$$e_{\alpha\beta} = \left[\begin{array}{c|c} 0 & \dfrac{\partial \Delta(\sigma^{**})}{\partial \sigma_i} \\ \hline \dfrac{\partial N_i(z^{**}, \sigma^{**})}{\partial z} & \dfrac{\partial N_i(z^{**}, \sigma^{**})}{\partial \sigma_i} \end{array}\right]. \qquad [19a]$$

Here X_α has the same components as σ_i, augmented with z, except that they refer to the coordinates centered on the singular points, namely

$$X_\alpha = \begin{bmatrix} z - z^{**} \\ \alpha_i - \sigma_i^{**} \end{bmatrix}. \qquad [19b]$$

We shall show, further, in Appendix C, that matrix $e_{\alpha\beta}$ possesses $n-1$ zero eigenvalues and two nonzero eigenvalues $\lambda_1 \neq \lambda_2$ which, generally speaking, have nonvanishing real parts in the nondegenerate case. This is a consequence of the fact that matrix $e_{\alpha\beta}$ operating on any vector in the manifold $\mathscr{S}$ of $n-1$ dimensions renders it equal to zero. It follows that the arbitrary vector is an eigenvector with zero eigenvalue. Consequently, there exist exactly two eigenvectors, regardless of the number n of nonlinear equations in [1], which define a plane. Thus, the types of singular points to be considered coincide with the elementary ones recalled at the beginning of this section and in figure 3.

The two eigenvalues are to be determined with the aid of the quadratic equation

$$\lambda^2 - \left(\sum_{\alpha=0}^{n} e_{\alpha\alpha}\right)\lambda + \sum_{0 \leqslant \alpha < \beta \leqslant n} (e_{\alpha\alpha} e_{\beta\beta} - e_{\alpha\beta} e_{\beta\alpha}) = 0. \qquad [20]$$

The above two eigenvalues produce two eigenvectors, say $\boldsymbol{\xi}$ corresponding to λ_1 and $\boldsymbol{\eta}$ corresponding to λ_2. The eigenvectors are embedded in Ω and are described by the $n+1$ components $\{\xi_0, \xi_1, \ldots, \xi_n\}$and $\{\eta_0, \eta_1, \ldots, \eta_n\}$ implied in the equations

$$\lambda_1 \xi_\alpha = e_{\alpha\beta} \xi_\beta \quad (\alpha, \beta = 0, 1, \ldots, n) \qquad [21a]$$

and

$$\lambda_2 \eta_\alpha = e_{\alpha\beta} \eta_\beta \quad (\alpha, \beta = 0, 1, \ldots, n). \qquad [21b]$$

The preceding represent two homogeneous systems of equations and their solutions define two characteristic directions $\boldsymbol{\xi}$ and $\boldsymbol{\eta}$ when λ_1 and λ_2 are real (saddle point or node). Numerical calculations in the neighborhood of a singular point must start with (z^{**}, σ^{**}) and include a first step along the above directions. Where λ_1 and λ_2 are complex conjugate, the singular point is a spiral (focus) and no trajectory can pass through it. The two directions [21a, b] together with the

†Matters can become more complex if cases with rank $A_{ij}(z^{**}, \sigma^{**}) \leqslant n-2$ were to be included, but we do not find it necessary to do so for reasons explained earlier.

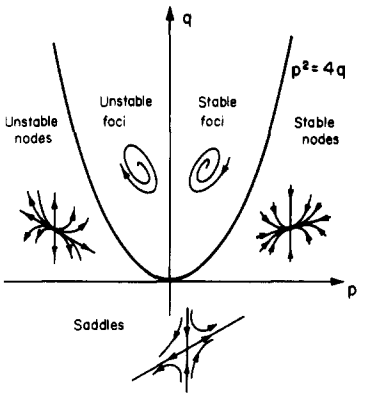

Figure 3. Classification of singular points $p = \lambda_1 + \lambda_2$, $q = -\lambda_1\lambda_2$.

trace $\Delta = 0$ provide us with a quantitative description of the trajectories in the neighborhood of (z^{**}, σ^{**}). The three topological patterns in question are discussed in more detail below.

6.5. Saddle points

We recall from [17] that saddle points occur when

$$\lambda_1 < 0 < \lambda_2. \qquad [22]$$

They are usually encountered just downstream of a throat in a convergent–divergent channel, and the two directions ξ and η in [21a, b] have opposite signs.

A saddle point $\mathscr{S}$ is illustrated with the aid of figure 4, which is drawn in the plane determined by the two eigenvectors ξ and η. The intersections $\Delta = 0$ and $N_1 = 0$ with this plane and the singular point $\mathscr{S}$ are also shown.

It is important to notice that at $\mathscr{S}$ itself the trajectories cross it with finite slopes, whereas at an infinitesimal distance from it, the tangent direction is either parallel or perpendicular to the z-axis. This is the reason for the severe difficulties that beset numerical calculations on the neighborhood of such points and for the impossibility of identifying them by numerical, forward integration.

It is clear from our earlier remarks that not all trajectories of figure 4 are acceptable as solutions of a physical problem. Referring to figure 5, which we interpret as a projection into the P, z plane, we see that the trajectories shown by —— lines solve a realizable initial-value problem.

The trajectories shown by —— lines pass through the saddle point (z^{**}, P^{**}) and, evidently, represent critical flow, i.e. flow choked at $z = z^{**}$. Starting with $P = P^{\circ}$ at $z = 0$, the trajectory

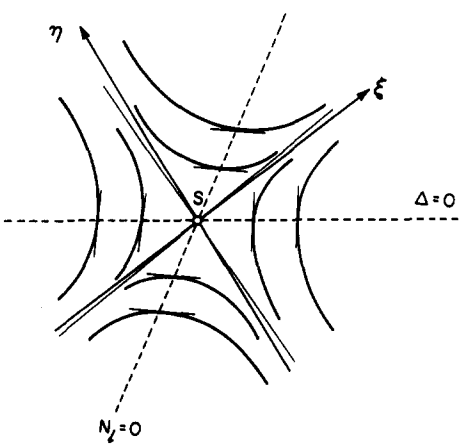

Figure 4. Saddle point in plane determined by the eigenvectors ξ and η.

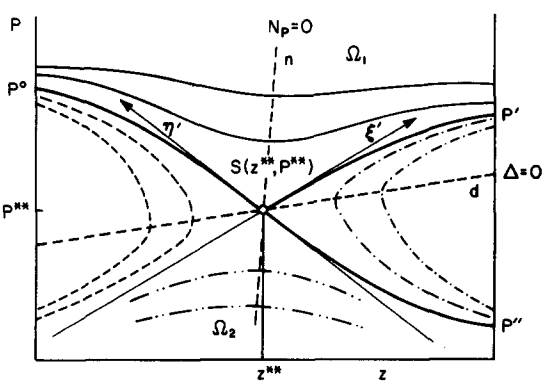

Figure 5. Physical interpretation of a saddle point.

progresses subcritically to the saddle point and then may proceed either with a continuous slope η' ending with P'' at $z = L$ or with a changed slope ξ' ending with P' at $z = L$. Here ξ' and η' are projections of ξ and η.

The line denoted by d represents the locus of the projections of turning points located on $\Delta = 0$, and line n represents the locus of the projections of the maxima and minima located on the trajectories as they cross $N_P = 0$. Along d we have $\Delta = 0$ and along n we have $N_P = 0$, as indicated. It should be noted that the line $\Delta = 0$ is not parallel to the z-axis, though the generators of hypercylinder $\mathscr{T}$ are, because the turning points on this set do not lie on a generator.

The trajectories shown by – – – lines, on the left of the figure, possess turning points and do not, therefore, represent acceptable solutions, except for appropriately truncated channels. Only their upper branches start with a subcritical velocity. The trajectories shown by —·— lines are physically meaningless.† The trajectories shown by —··— lines start in Ω_2 and fall outside the scope of problems of interest in this paper.

The topological pattern of figure 5 allows us to recognize that flows with initial pressures $> P^\circ$ end with pressures $> P'$. For such flows, the exit conditions are completely determined by the inlet conditions. Flows starting with P° may branch out at $\mathscr{S}$, and the decision as to which branch is followed subsequently now depends on the back-pressure P' or P'', respectively. It must be recognized that flows with exit pressure $P'' < P_e < P'$ and $P_e < P''$ are not described by our mathematical model at all. To include them in the analysis it is necessary to supplement the mathematical model with additional physical considerations. In particular, it is clear on physical grounds that flows with $P_e < P''$ must expand outside the channel, and that some of the flows with $P'' < P_e < P'$ must develop more intense entropy production rates than are implied in b_j. These may be produced by shock waves or extended zones of enhanced dissipation.

6.6. Nodal points

The pattern of a nodal point is shown in figure 6. Such points seem to occur only rarely, and we do not find it necessary to provide a detailed discussion, because the interpretation should now be clear to the reader by analogy with subsection 6.5. More precisely, the pattern has been drawn in the plane determined by ξ and η, and lines $\Delta = 0$, $N_1 = 0$, $N_2 = 0$ are lines of intersection of the respective manifolds with the plane of the drawing. We merely add as a matter of curiosity that such points were identified by Kestin & Zaremba (1954) in the flow of a gas through a tube rotating about a vertical axis (helicopter feedline to propeller).

6.7. Spirals (foci)

The pattern which accompanies a spiral is drawn in figure 7, which is analogous to figures 4 and 6. Such points, too, do not appear very frequently. In one case reported by Kestin & Zaremba (1953), the spiral point followed a saddle point, as shown in figure 8, and was due to an inflection point in the divergent portion of the nozzle profile. Spirals cross the line $\Delta = 0$ at many points, which represent turning points, and the interpretation of this fact is now clear. For example, in figure 8 the trajectory shown by —— lines represents a flow which is choked twice, first inside the channel at z_1^{**} and secondly at the end of it, assuming that the channel length is L_1. In a channel of length L_2, the flow cannot choke at z_1^{**}, but does so at L_2, owing to the effect of the focus at z_2^{**}.

Spiral points have also been reported by Kestin & Mikielewicz (1982) in their study of two-phase flow down a pipe in a vertical gravitational field (geothermal rejection well).

7. CONSTANTS OF THE MOTION

In some models it is possible to integrate one (or more) conservation equation in closed terms. This is the case, for example, when steady-state adiabatic flow is analyzed with the aid of the homogeneous model. Such an integral leads to the identification of a quantity which remains constant along a particular set of trajectories, though not along all of them. In dynamics, this

†We know from gas dynamics that they may acquire some physical significance if shock waves appear, but we do not wish to discuss such cases in this paper.

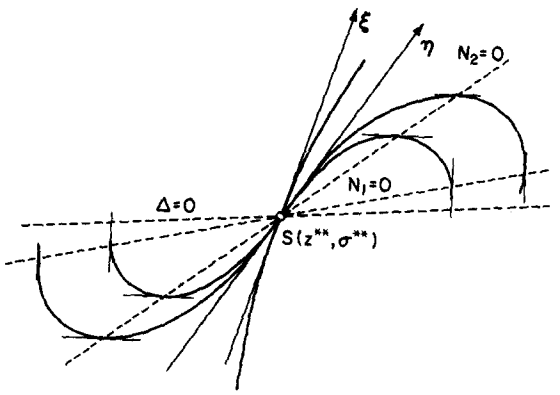

Figure 6. Nodal point.

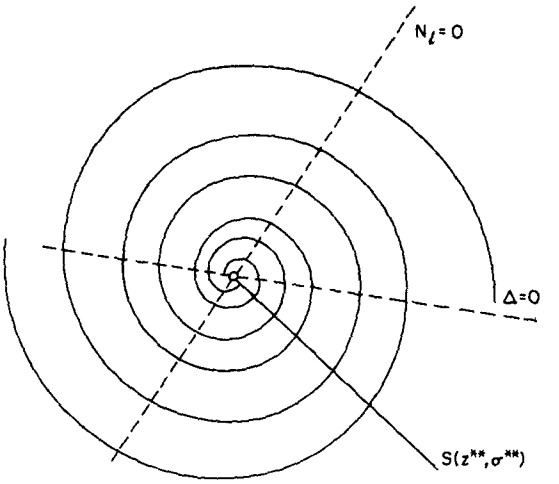

Figure 7. Spiral (focus).

quantity is known as "the constant of the motion". When this is the case it is possible, and usually desirable, to parametrize the problem and to regard the phase space Ω of $n+1$ dimensions as a union of an infinite set of spaces each of n dimensions only, each constituting a set of trajectories characterized by a common value of the "constant of the motion".

The advantage of this procedure is that now the topological study is conducted in a space of lower dimensionality.

8. LOCATION OF SINGULAR POINT

In steady flows, the shape of the channel always enters the vector b_j through the equation of mass conservation for the mixture which can be put in the form

$$\frac{1}{\rho}\frac{\mathrm{d}\rho}{\mathrm{d}z}+\frac{1}{w}\frac{\mathrm{d}w}{\mathrm{d}z}=-\frac{\mathrm{d}\ln A(z)}{\mathrm{d}z}. \qquad [23]$$

Thus the term $\mathrm{d}\ln A(z)/\mathrm{d}z$ appears in one of the two equations which define a singular point. Explicitly, these are

$$\Delta(\sigma)=0 \text{ and } N_i\left[z,\sigma;\frac{\mathrm{d}\ln A(z)}{\mathrm{d}z}\right]=0. \qquad [24]$$

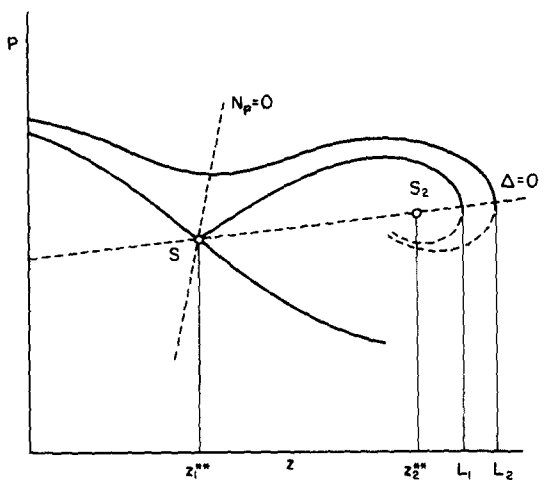

Figure 8. Spiral following a saddle point.

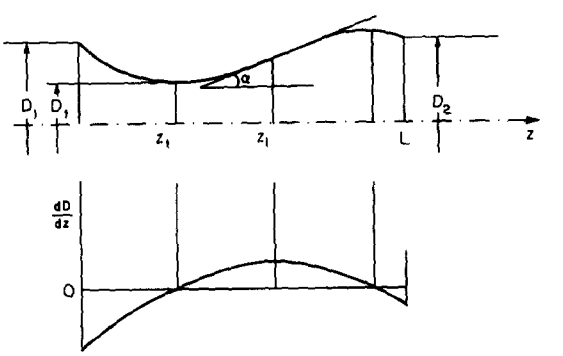

Figure 9. Selected nozzle shape, $D(z)$, and its slope $\mathrm{d}D/\mathrm{d}z$; $D_1=0.2$ m, $D_2=0.2$ m, $D_t=0.1$ m, $z_t=0.25$ m, $z_i\cong 0.42$ m, $L=0.8$ m, $\alpha=15°$.

It follows that the location of the singular point along the channel axis is determined by solving for $\mathrm{d} \ln A(z)/\mathrm{d}z$. The pair [24] is a system of two simultaneous algebraic equations each in $n+1$ variables, leaving $n-1$ of them undetermined. When $n=2$, and the system is parametrized, we obtain a unique value of z^{**} for every value of the parameter. The location of a singular point thus turns out to be coordinated with the state σ^{**} at it, and is not a general characteristic of the shape of the channel.

9. AN EXAMPLE

The purpose of this and the following sections is to apply the geometric method to the analysis of flow through a channel of varying cross section. The channel shape chosen for the analysis is shown in figure 9. For reasons that will be explained later, the nozzle profile has been provided with a point of inflection at z_i. Thus, the derivative $\mathrm{d}A/\mathrm{d}z$ passes through zero at $z=z_t$, attains a maximum at $z=z_i$ and then decreases, passing through zero once more at $z<L$.

The choice of the mathematical model for this illustration presented us with some difficulties. On the one hand, we are aware of the importance of certain physical phenomena in their effect on choking. These include the need to predict the point of flashing if it occurs inside the channel (Réocreux 1974; Saha *et al.* 1982) and, even more importantly, to account for supersaturation (subcooling) in the liquid phase (onset of thermodynamically metastable states). At the present time there exist no proven and generally accepted models which account for such phenomena. Similarly, the general question of appropriate closures is also unresolved (Bouré 1986). For these reasons we must defer an analysis of a proven mathematical model to a future date. Rather, we opt for the simplest homogeneous equilibrium model. This choice is not completely unrealistic, because (Henry 1981) it has been established that such models seem to be useful when applied to the study of choking at comparatively large values of quality, say at void fractions $\alpha > 0.7$ or so. This model has, furthermore, been successfully employed on the design of the low-pressure stages of steam turbines over many years.

An additional reason for being satisfied with the simplest, not to say simplistic, model is the contention that the description of choking should emerge naturally as a characteristic of the mathematical model, and this simple choice will enable us to display the essential features of the analysis with a minimum of distraction.

10. THE MODEL

We use the term "model" as encompassing the conservation laws, the closure conditions and the equation of state of the fluid, here consisting of water and steam for definiteness. We direct attention towards the homogeneous, adiabatic equilibrium model which uses the following three conservation laws:

$$\frac{\mathrm{d}}{\mathrm{d}z}(A\rho w)=0; \qquad [25a]$$

$$\frac{\mathrm{d}P}{\mathrm{d}z}+\rho w\frac{\mathrm{d}w}{\mathrm{d}z}+\frac{C\tau_w}{A}=0; \qquad [25b]$$

and

$$\frac{\mathrm{d}}{\mathrm{d}z}(h+\tfrac{1}{2}w^2)=0. \qquad [25c]$$

The symbol z denotes the physical length coordinate measured along the flow axis, $A(z)=\pi[D(z)]^2/4$ is the variable cross-sectional area of the channel, w is the velocity, ρ is the density, P is the pressure and h is the enthalpy; the shearing stress τ_w at the wall is written as

$$\tau_w=\frac{1}{2}f\rho w^2 \quad (f=0.008=\text{const}) \qquad [26]$$

and the equation of state of thermodynamic equilibrium,

$$\rho = \rho(h, P), \tag{27}$$

is fully defined in the *Steam Tables* (Haar *et al.*, 1984).

11. THE PROBLEM

The specific problem is to determine all possible categories of solutions of flows when the inlet stagnation condition is in the two-phase region and the back-pressure is progressively reduced from that at the inlet down to the range where the mass flow rate $\dot{m}$ has attained its largest value and has become insensitive to the back-pressure.

The particular nozzle, shown in figure 9, has the following dimensions: $D_1 = 0.2$ m at $z = 0$; $D_2 = 0.2$ m at $z = L = 0.8$ m; $D_t = 0.1$ m at $z_t = 0.25$ m with the slope $\alpha = 15°$ at the inflection point.

The profile consists of two parabolas, one with its minimum at z_t, the other with its maximum at $z < L$, both tangential to each other at $z = 0.42$ m. The variation of the slope dD/dz is shown underneath the profile.

Equation [25c] integrates immediately to

$$h + \tfrac{1}{2} w^2 = h_0 \tag{25d}$$

and allows us to employ the stagnation enthalpy h_0 ("constant of the motion") to parametrize the system [25a–c]. Consequently, our model equations acquire the simplified form:

$$\frac{C_1}{\rho}\frac{dP}{dz} - \left[\frac{1}{2(h_0 - h)} - \frac{C_2}{\rho}\right]\frac{dh}{dz} = -\frac{2D'}{D}; \tag{28a}$$

$$\frac{dP}{dz} - \rho\frac{dh}{dz} = -\frac{4f\rho(h_0 - h)}{D}; \tag{28b}$$

and

$$\frac{dh_0}{dz} = 0. \tag{28c}$$

Here

$$C_1 = \left(\frac{\partial \rho}{\partial P}\right)_h > 0, \quad C_2 = \left(\frac{\partial \rho}{\partial h}\right)_P < 0. \tag{28d, e}$$

The derivatives C_1 and C_2 retain the given signs over most of the area of interest in the two-phase portion of the h, P diagram (Rivkin *et al.* 1978).

The preceding system can be described in the 2-D state space h, P with $h_0 = \text{const}$ playing the role of a variable parameter. The model now assumes the canonical form

$$A_{ij}(\sigma)\frac{d\sigma_i}{dz} = b_j(\sigma, z), \tag{29}$$

with h and P constituting the components of the dependent vector σ.

The analysis will be conducted in the phase space $\Omega\{P, h, z;\ h_0 = \text{const}\}$, where

$$A_{11} = \frac{C_1}{\rho}, \qquad A_{12} = -\tfrac{1}{2}(h_0 - h) + \frac{C_2}{\rho}, \tag{30a, b}$$

$$A_{21} = 1, \qquad A_{22} = -\rho, \tag{30c, d}$$

$$b_1 = \frac{-2D'}{D}, \quad b_2 = \frac{-4f\rho(h_0 - h)}{D}. \tag{30e, f}$$

Owing to parametrization, we can represent the "portrait" of the trajectories in a space of only three dimensions.

12. SOLUTION

The solution of the problem consists of the setting up of an algorithm for the calculation of pressure and enthalpy distributions along the channel for a given pair of stagnation values, P_0 and h_0, ahead of the inlet ($z = 0$). We employ the methodology of sections 2–8 and supplement the mathematical discussion with an analysis of the physical acceptability of trajectories and the quantitative features of choking.

The autonomous equivalent of [25a–c] is

$$\frac{d\sigma_i}{dt} = N_i, \quad \frac{dz}{dt} = \Delta \quad (i = P, h), \tag{31a, b}$$

with t denoting an arbitrary parameter. Here

$$\Delta = \det(A_{ij}) = -\left[C_1 - \frac{C_2}{\rho}\right] + [2(h_0 - h)]^{-1}, \tag{32a}$$

$$N_P = \frac{4f(h_0 - h)C_2}{D} - 2f\frac{\rho}{D} + \frac{2D'\rho}{D} \tag{32b}$$

and

$$N_h = -\frac{4C_1 f(h_0 - h)}{D} + 2\frac{D'}{D}, \tag{32c}$$

where $D' = dD/dz$.

We recall that the quantities Δ, N_P and N_h are interpreted as components of the directional vector V which is everywhere tangential to a trajectory m in the phase space, figure 10. This would enable us to use the geometric method of isoclines and to sketch the set of trajectories. However, nowadays, the preferred method is one of numerical integration. We further recall that through all regular points $\sigma_i^\circ(h^\circ, P^\circ)$, where $\Delta(h^\circ, P^\circ) \neq 0$, there passes one and only one trajectory which solves [25a–c] or [31a, b] without necessarily constituting an acceptable solution from the physical point of view. Any numerical scheme goes through smoothly if all points along a given trajectory are regular ones.

Numerical difficulties appear when $\Delta = 0$; at such points we either have

$$\Delta = 0, \quad N_h \neq 0, \quad N_P \neq 0 \text{ (turning points } \{h^*, P^*; z^*\}) \tag{33a}$$

or

$$\Delta = 0, \quad N_h = N_P = 0\dagger \text{ (singular points } \{h^{**}, P^{**}; z^{**}\}). \tag{33b}$$

The condition

$$\Delta = -\left[C_1 - \frac{C_2}{\rho}\right] + [2(h_0 - h)]^{-1} = 0 \tag{34}$$

proves that at all points of the cylinder $T(\Delta = 0)$, the flow velocity is

$$w^{*2} = 2(h_0 - h) = \frac{\rho}{C_1\rho + C_2}, \tag{35a}$$

which is equivalent to

$$w^* = a = \left[\frac{1}{\rho}\left(\frac{\partial\rho}{\partial h}\right)_P + \left(\frac{\partial\rho}{\partial P}\right)_h\right]^{-\frac{1}{2}} = \left[\left(\frac{\partial P}{\partial\rho}\right)_s\right]^{\frac{1}{2}}. \tag{35b}$$

Hence it follows that our adopted model implies that at all turning and singular points the local flow velocity is equal to the velocity of propagations of small plane disturbances.

†The case $\Delta = 0$ with only one N_i vanishing is impossible.

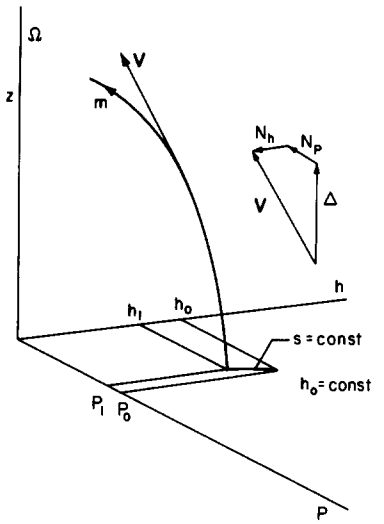

Figure 10. Typical trajectory m in phase space Ω showing directional vector V and its components Δ, N_P, N_h.

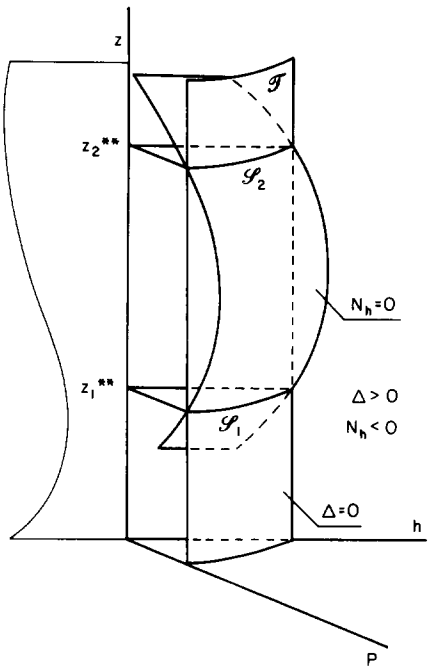

Figure 11. The loci $\mathscr{S}_1$ and $\mathscr{S}_2$ of singular points.

In order to understand the nature of the numerical difficulties it is useful now to identify the singular points. A knowledge of the location and character of the singular points permits us at the same time to draw the "portrait" of the trajectories in the phase space $\Omega\{h, P, z\}$ for each $h_0 = \text{const}$ and to assess the physical acceptability of the various categories of trajectories.

13. SINGULAR POINTS

The manifold $\mathscr{S}$ of all singular points satisfies two conditions. In addition to [34], we choose

$$N_h = -\frac{4C_1 f(h_0 - h)}{D} + \frac{2D'}{D} = 0. \qquad [36a]$$

This is equivalent to

$$D' = 2C_1 f(h_0 - h) \quad (>0), \qquad [36b]$$

whose r.h.s. is always positive ($h_0 > h$).

The preceding result proves that critical flow can set in only in the divergent portion of the nozzle. As far as the channel shown in figure 9 is concerned, singular points can occur both downstream of z_t, say at z_1^{**}, as well as at z_2^{**} past z_t.

The two singular points must lie on curves $\mathscr{S}_1$ and $\mathscr{S}_2$ which result from the intersection of the surface $\Delta = 0$ with the surface $N_h = 0$, shown in figure 11. Our numerical studies suggest that the loci $\mathscr{S}_1$ and $\mathscr{S}_2$ are practically at right angles to the z-axis, as indicated in the figure. This proves that the locations z_1^{**} and z_2^{**} of the two critical cross sections in the nozzle are insensitive to the values of P^{**} and h^{**} which satisfy $\Delta = 0$.

It has been proved previously that trajectories which solve the system [31a, b] can pass only through a saddle point or a nodal point. Should any singular point turn out to be a spiral, which possesses no real characteristic directions, it will be known that no trajectory can pass through it. We shall then be dealing with a straightforward initial-value problem whose numerical solution will encounter no obstacles.

In what follows, we concentrate on saddle points and nodal points. In such cases, a numerical procedure must start with the singular point rather than with the inlet.

Equations [34] and [36b], taken singly, have proved that the velocity at a critical cross section must be sonic and that such a section can occur only in the divergent portion of the channel. Taken together, they are insufficient uniquely to determine the relevant velocity vector $\mathbf{V}(P^{**}, h^{**}, z^{**})$. First, we need three relations, and secondly we must relate the three parameters to the values P_0, h_0 at the upstream stagnation point. The point P_0, h_0 in figure 10 is linked to P_1, h_1 by $s = \text{const}$. The pressure P_0 does not appear explicitly in the equations, even though h_0 is supposedly known. It is clear that $\mathbf{V}^{**}$ must satisfy [31a, b] and that, consequently, P_0 must be computed iteratively by reverse integration.

We begin by assuming a value P^{**}, say $P^{**(1)}$, which together with [34] and [36b] specify $\mathbf{V}^{**(1)}$. In practice it is recommended to put $P^{**(1)} = (0.6 - 0.8)P_0$. The first step in the reverse integration cannot be taken on the basis of [31a, b] for the reasons explained previously. This must progress along an eigendirection. The next steps follow [31a, b].

The character of the singular point and the eigendirections (for each assumed value $P^{**(1)}$) are calculated with the aid of the linearized form

$$\frac{dX_i}{dt} = e_{ij}X_j, \tag{37a}$$

where X_i has components

$$X_1 = P - P^{**}, \quad X_2 = h - h^{**}, \quad X_3 = z - z^{**} \tag{37b}$$

and

$$e_{ij} = \begin{bmatrix} \dfrac{\partial N_P^{**}}{\partial z} & \dfrac{\partial N_P^{**}}{\partial h} & \dfrac{\partial N_P^{**}}{\partial P} \\ \dfrac{\partial N_h^{**}}{\partial z} & \dfrac{\partial N_h^{**}}{\partial h} & \dfrac{\partial N_h^{**}}{\partial P} \\ \dfrac{\partial \Delta^{**}}{\partial z} & \dfrac{\partial \Delta^{**}}{\partial h} & \dfrac{\partial \Delta^{**}}{\partial P} \end{bmatrix}. \tag{37c}$$

Explicit forms of the elements of e_{ij} in our case are seen listed in table 1. The character of the singular point depends on the eigenvalues of e_{ij}, and the characteristic eigendirections follow the eigenvectors. The integration is terminated at $z = 0$, and the resulting value $P_0^{(1)}$ is compared with

Table 1. Elements of the linearized matrix e_{ij}

$$\frac{\partial \Delta}{\partial P} = -\frac{\partial C_1}{\partial P} + \frac{C_2 C_1}{\rho^2} - \frac{1}{\rho}\frac{\partial C_2}{\partial P}$$

$$\frac{\partial \Delta}{\partial h} = -\frac{\partial C_1}{\partial h} + \frac{1}{2(h_0 - h)^2} - \frac{1}{\rho^2}\left(\rho\frac{\partial C_2}{\partial h} + C_2^2\right)$$

$$\frac{d\Delta}{\partial z} = 0$$

$$\frac{\partial N_P}{\partial P} = \frac{2D'}{D}C_1 + \frac{4f(h_0 - h)}{D}\frac{\partial C_2}{\partial P} - \frac{2f}{D}C_1$$

$$\frac{\partial N_P}{\partial h} = \frac{2D'}{D}C_2 + \frac{4f}{D}\left[(h_0 - h)\frac{\partial C_2}{\partial h} - C_2\right] - \frac{2f}{D}C_2$$

$$\frac{\partial N_P}{\partial z} = 2\rho\frac{D''D - D'^2}{D^2} - \frac{D'}{D^2}\left[4f(h_0 - h)C_2 - 2f\rho\right]$$

$$\frac{\partial N_h}{\partial P} = -\frac{4f(h_0 - h)}{D}\frac{\partial C_1}{\partial P}$$

$$\frac{\partial N_h}{\partial h} = -\frac{4f}{D}\left[\frac{\partial C_1}{\partial h}(h_0 - h) - C_1\right]$$

$$\frac{\partial N_h}{\partial z} = \frac{4C_1 f(h_0 - h)D'}{D^2} + 2\frac{D''D - D'^2}{D^2}$$

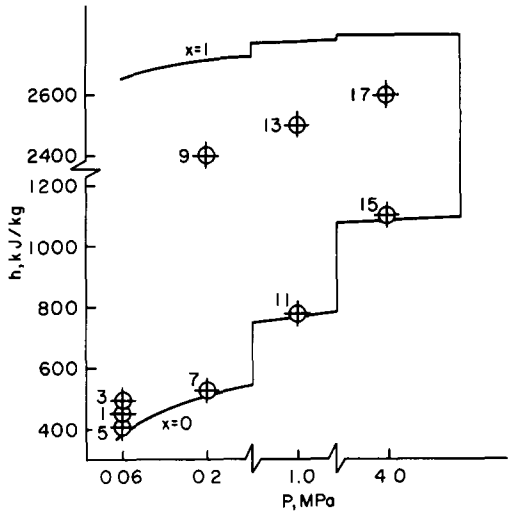

Figure 12. States in the h, P state plane used in the survey of table 2.

the given P_0, and iterated, if necessary. The iteration ends for $|P_0 - P_0^{(1)}| < \epsilon$, where ϵ is the acceptable uncertainty in P_0.

14. NUMERICAL EXAMPLES

We have performed a survey of singular points and characteristic directions for the nozzle specified earlier. In all cases, the critical points were located in the wet region, see figure 12. The results are listed in table 2. Here, we have imposed values of the stagnation enthalpy, h_0, and *assumed* values of the critical pressure $P_1^{**} = P_2^{**}$, looking for the character, and exact location,

Table 2. Survey of singular points for the numerical example

No.	P^{**} (MPa)	h_0 (kJ/kg)	x^{**}	w^{**} (m/s)	z^{**} (m)	Type of singular point	$\frac{dP}{dz^{**}}$ (Pa/m)	$\frac{dh}{dz^{**}}$ (J/m)
1	0.06	400	0.0174	29.1	0.25255	Saddle	−169008	−8173
							+161073	+8053
2	0.06	400	—	—	0.675156	Spiral	—	—
3	0.06	500	0.0597	78.4	0.252611	Saddle	−257382	−41751
							+248749	+42284
4	0.06	500	—	—	0.675012	Spiral	—	—
5	0.06	362	0.0011	2.7	0.252505	Saddle	−55715	−224
							+48312	+196
6	0.06	362	—	—	0.675178	Spiral	—	—
7	0.20	506	0.0009	3.6	0.252507	Saddle	−201679	−381
							+176320	+337
8	0.20	506	—	—	0.675175	Spiral	—	—
9	0.20	2500	0.8638	415.8	0.252726	Saddle	−1247230	−932797
							+1214912	+963215
10	0.20	2500	—	—	0.674833	Spiral	—	—
11	1.00	764	0.0013	10.1	0.252518	Saddle	−1475292	−2020
							+1341486	+1868
12	1.00	764	—	—	0.675159	Spiral	—	—
13	1.00	2600	0.8681	432.9	0.252767	Saddle	−6230648	−1014057
							+6069525	+1047036
14	1.00	2600	—	—	0.674769	Spiral	—	—
15	4.00	1092	0.0002	28.8	0.252546	Saddle	−8484462	−10612
							+7965449	+10220
16	4.00	1092	—	—	0.675114	Spiral	—	—
17	4.00	2700	0.8862	438.8	0.252809	Saddle	−24589560	−1052294
							+23949028	+1085698
18	4.00	2700	—	—	0.674703	Spiral	—	—

of the singular points near z_t and z_1, respectively. It is seen that the former always turned out to be a saddle, whereas the latter was a spiral. This was done in the interest of saving computing time, even though it is realized that points with equal values of P^{**} and h_0 correspond to different values of P_0—not computed for the 18 listed cases. However, the dryness fraction x^{**} was listed for all saddle points. Here it is necessary to remember that no trajectory passes through a spiral point; hence no values of the dryness fraction or velocity were assigned to them. As is usual in steam-turbine practice, the dryness fraction is the local mass ratio of vapor to the sum of vapor and liquid.

Complete calculations were executed for

$$\text{(a) } P_0 = 0.09 \text{ MPa}, \quad h_0 = 500 \text{ kJ/kg},$$

$$\text{(b) } P_0 = 1.5 \text{ MPa}, \quad h_0 = 1000 \text{ kJ/kg}.$$

The resulting portraits projected into the P, z plane are shown in figures 13 and 14. In both cases a saddle point S_1 is followed by a spiral S_2. In this projection, the singular points lie at the intersection of two curves labeled $\Delta = 0$ and $N_P = 0$. The former is the locus of all turning points for the given h_0. The latter is the projection of the loci $\mathscr{S}_1$ and $\mathscr{S}_2$ where both $\Delta = 0$ and $N_P = 0$. The insensitivity of the location of the singular-point cross sections to the thermodynamic state appears clearly. In particular, we find that:

$$\text{in case (a)}, \quad \frac{P_1^{**}}{P_0} = \frac{P_2^{**}}{P_0} = 0.704;$$

$$\text{in case (b)}, \quad \frac{P_1^{**}}{P_0} = \frac{P_2^{**}}{P_0} = 0.700.$$

Trajectories 1–3 have been obtained by reverse and forward integration, as the case may be, the first directions being determined along the eigenvectors v_1 and v_2. Trajectory 4 starts with a supercritical inlet condition, and is of no interest in this paper.

The trajectories in area A all pass through regular points and correspond to physically acceptable flows. The curves with turning points in area B do not correspond to physically acceptable solutions, unless truncation of the nozzle ahead of z_1 is contemplated. Trajectory 1–2 corresponds to the highest back-pressure P' at which the flow has become choked. Trajectory 1–3 determines

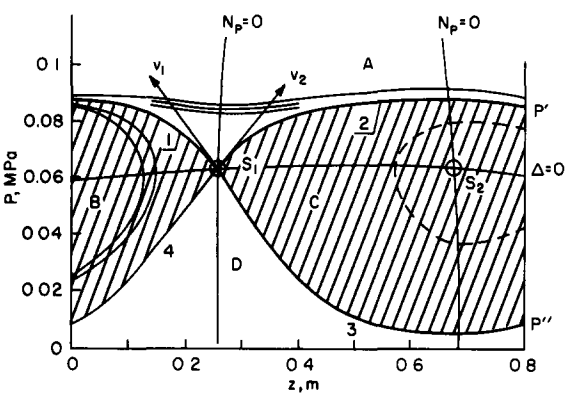

Figure 13. Categories of trajectories; $P_0 = 0.09$ MPa, $h_0 = 500$ kJ/kg. $\Delta = 0$ denotes the locus of turning points; $N_P = 0$ denotes the locus $N_P = 0$; A, all subcritical trajectories; B, impossible trajectories in the given nozzle; C, solutions of model equations do not give physically acceptable solutions; D, solutions of model equations do not give physically acceptable solutions to problem analyzed in this paper; 1–2, choked flow with all velocities in the subcritical region; 1–3, choked flow with transition from subcritical to supercritical flow; S_1, saddle point; S_2, spiral point.

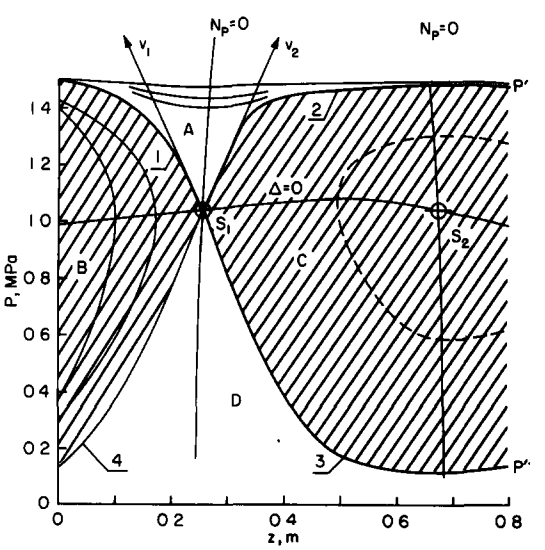

Figure 14. Categories of trajectories: $P_0 = 1.5$ MPa, $h_0 = 1000$ kJ/kg. Notation as in figure 13.

the second back-pressure P'' at which choked flow represents a solution of [31a–c]. Area C contains trajectories with turning points, one of which is shown. Such trajectories are solutions of [31a–c], but are deprived of physical significance in the present context. It is clear that trajectories which emanate from S_1 and branch out from trajectory 3, ending with back-pressure $P'' < P_a < P'$, are physically possible, but they would not be solutions of [31a–c]. On the basis of experimental observations it can be asserted that the flow along these trajectories must occur with increased entropy production compared to that built into the original model. This may be caused by shock waves, separation and other observable dissipative mechanisms. For pressures $P_s < P''$, the flow follows the trajectory 1–3.

We have disregarded the trajectories in the supercritical area D as lying outside the area of interest of this paper.

In summary, we can make the following statements regarding flows with decreasing back-pressure P_a.

$P' < P_a < P_0$ (area A): flows with decreasing mass flow rate $\dot{m}$; trajectories possess physical significance and are obtained numerically without difficulty; all states are subcritical.

$P_a = P'$: first onset of choking; trajectories 1 and 2 require special treatment in computer program.

$P'' < P_a < P'$ (area C): trajectories which are mathematical solutions of the adopted model do not constitute physically acceptable solutions.

$P_a = P''$: second onset of choking with subcritical branch 1 and supercritical branch 3; special treatment of numerical scheme required.

$0 < P_a < P''$: flow occurs along trajectory 1–3; mathematical solutions in area D do not constitute physical solutions of our problem.

As far as inlet conditions are concerned, the analysis shows that in the prescribed circumstances this nozzle cannot develop pressure $P < \bar{P}$ at the inlet. In our examples,

$$\text{(a) } \bar{P} = 0.0889 \text{ MPa}, \quad \text{(b) } \bar{P} = 1.489 \text{ MPa}.$$

15. CONICAL NOZZLES AND CYLINDRICAL CHANNELS

Nozzles whose profiles contain a conical divergent portion or a conical convergent as well as a divergent portion have been used in experimental research because they are comparatively easy to manufacture. They also deserve attention from the computational point of view because for them $D' = K$ is a constant. Nozzles consisting of two cones with the throat at their juncture, with or without a fillet of small radius (e.g. Réocreux 1974; Saha *et al.* 1982) present particular difficulties, because the function $D'(z)$ is not smooth and changes sign at the throat. We shall not consider such cases in this paper and only discuss smooth nozzles with a conical divergent portion, as shown in figure 15. We assume that the saddle point happens to be located in the conical section downstream from the fillet, i.e. with

$$D' = K = 2C_1 f(h_0 - h) \quad (>0) \qquad [38]$$

in [36b]. Reference to [36a] shows that the equation has now ceased to contain any explicit functions of z. The situation that has arisen in the phase space $\Omega(P, h, z)$ is depicted in figure 16. The surfaces $N_h = N_P = \Delta = 0$ intersect along a line $\mathcal{T}$ which is parallel to the z-axis. Consequently, the state h^{**}, P^{**} is uniquely determined and is the same for all possible locations of the critical cross section; it follows as a solution of the simultaneous equations [34] and [36a] with $D' = K$.

In order to determine the location z_1^{**} it is now necessary to integrate forward, and to bracket

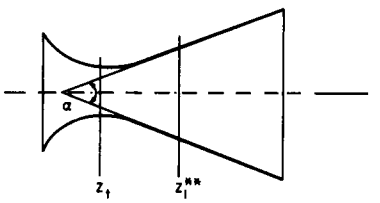

Figure 15. Smooth nozzle with a conical divergent portion and a saddle point located in it.

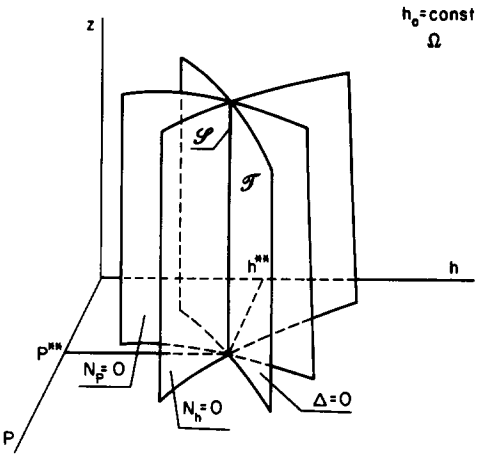

Figure 16. Phase space for the conically diverging portion of a nozzle.

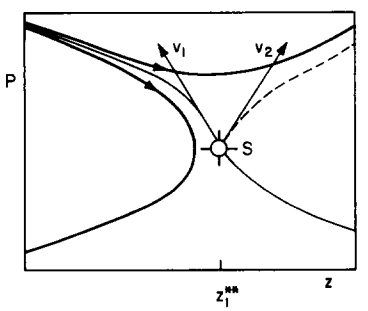

Figure 17. Bracketing the location of the critical cross section with the conical divergent portion.

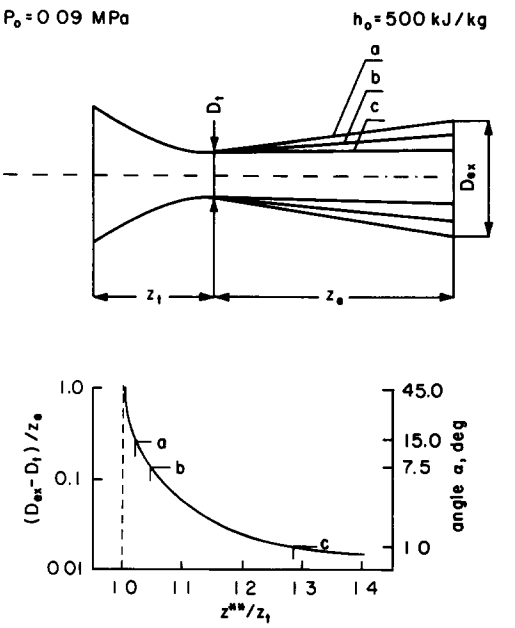

Figure 18. Set of nozzles with varying conical divergent portions, and movement of the critical cross section, depending on the angle of the cone.

the critical solution with two close surves (figure 17), one with a minimum in P, h, and the other a turning point.† The analytically calculated values of h^{**} and P^{**} serve as a very useful check.

It should be noted that in the case of a cylindrical pipe of constant cross section, D′ vanishes in [36a]. Consequently, N_h is always negative and cannot vanish. In this case, as shown previously (Bilicki & Kestin 1983), all trajectories acquire turning points and the singular point recedes to $z \to \infty$. With D′ = K, as in a cone, N_h can become equal to zero if D′ is just large enough. This suggests that varying the angle of divergence α of a conical channel must ultimately have a large effect on the locations z_1^{**} of the critical cross section. This will occur near that value of D′ which just makes it possible for N_h to vanish. Such a situation is illustrated in figure 18 which depicts

†Note that the appearance of two such curves with only slightly different initial conditions *does not signify that the computer program diverges.*

the location z^{**}/z_t as a function of the angle α and opening $(D_{ex} - D_t)/z_e$. The location becomes very sensitive to the angle below about $\alpha = 7°$.

Acknowledgements—The work described in this paper is an elaboration of Report NUREG/CR-3695, originally completed under Grant No. NRC-G-04-83-013[3] awarded by the Nuclear Regulatory Commission to Brown University. The subsequent work was supported by the Office of Energy Engineering Research of the U.S. Department of Energy under Grant DE-AC02-84ER-13167.

The authors express their appreciation to M. M. Pratt for his critical reading of the manuscript.

REFERENCES

ARNOLD, V. I. 1973 *Ordinary Differential Equations*. MIT Press, Cambridge, Mass.

ARNOLD, V. I. 1978 *Mathematical Methods of Classical Mechanics*. Springer, New York.

ARNOLD, V. I. 1982 *Geometrical Methods in the Theory of Ordinary Differential Equations*. Springer, New York.

BILICKI, Z. & KESTIN, J. 1983 Two-phase flow in a vertical pipe and the phenomenon of choking: homogeneous diffusion model—I. Homogeneous flow models. *Int. J. Multiphase Flow* **9**, 269–288.

BOURÉ, J. A. 1977 The critical flow phenomenon with reference to two-phase flow and nuclear reactor systems. In *Symposium on the Thermal and Hydraulic Aspects of Nuclear Reactor Safety, 1: Light Water Reactors* (Edited by JONES, O. C. JR & BANKOFF, S. G.), pp. 195–216. ASME, New York.

BOURÉ, J. A. 1986 Two-phase models: the closure issue. In *Multiphase Science and Technology: Bases of Modeling of Two-phase Systems* (materials arising from the *Workshop on Two-phase Flow Fundamentals*, Gaithersburg, Md, 1985), Part B, Chap. 1 (Edited by HEWITT, G. F., DELHAYE, J. M. & ZUBER, N.).

BOURÉ, J. A., FRITTE, A. A., GIOT, M. M. & RÉOCREUX, M. L. 1976 Highlights of two-phase critical flow: on the links between maximum flow rates and transfer phenomena in single and two-phase flow. *Int. J. Multiphase Flow* **3**, 1–22.

CODDINGTON, E. A. & LEVINSON, N. 1955 *Theory of Ordinary Differential Equations*. McGraw-Hill, New York.

DELHAYE, J. M., GIOT, M. & RIETHMULLER, M. L. 1981 *Thermohydraulics of Two-phase Systems for Industrial Design and Nuclear Engineering*. Hemisphere, Washington, D.C.

GUCKENHEIMER, J. & HOLMES, P. 1983 *Dynamical Systems and Bifurcations of Vector Fields*. Springer, New York.

HAAR, L., GALLAGHER, J. S. & KELL, G. S. 1084 *NBS/NRC Steam Tables*. Hemisphere, Washington, D.C.

HALE, J. K. 1969 *Ordinary Differential Equations*. Wiley, New York.

HENRY, R. E. 1981 Calculational techniques for two-phase critical flow. In *Two-phase Flow Dynamics* (Edited by BERGLES, A.. E. & ISHIGAI, S.). Hemisphere, Washington, D.C.

KAPLAN, W. 1958 *Ordinary Differential Equations*. Addison–Wesley, Reading, Mass.

KESTIN, J. & MIKIELEWICZ, J. 1982 Two-phase flow in a vertical pipe and the phenomenon of choking: homogeneous diffusion model—II. The case of downflow. Brown Univ. Report GEOFLO 14, LA-UR-82-1625. This report has now been replaced by the paper: BLICK, Z., KESTIN, J. & MIKIELEWICZ, J. 1987 Two-phase downflow in a vertical pipe and the phenomenon of choking; homogeneous diffusion model. *Int. J. Heat Mass Transfer*. Accepted for publication.

KESTIN, J. & ZAREMBA, S. K. 1952 Geometrical methods in the analysis of ordinary differential equations. *Appl. scient. Res. Math.* **B3**, 149–189.

KESTIN, J. & ZAREMBA, S. K. 1953 One-dimensional high-speed flows. *Aircr. Engng* **25**, 1–5.

KESTIN, J. & ZAREMBA, S. K. 1964 Adiabatic one-dimensional flow of a perfect gas through a rotating tube of uniform cross-section. *Aeronaut. Q.* **4**, 373–399.

PERRY, A. E. 1984 A study of degenerate and nondegenerate critical points in three-dimensional flow fields. Report DFVLR-FB84-36, Göttingen.

POINCARÉ, H. 1880–1890 *Mémoire sur Les Courbes Definés par Les Equations Differentielles I–VI*, Oeuvre I, Gauthier–Villars, Paris.

POINCARÉ, H. 1890 Sur les equations de la dynamique et le problème de trois corps. *Acta math., Stockh.* **13**, 1–270.

POINCARÉ, H. 1899 *Les Methodes Nouvelles de la Mécanique Celeste.* Gauthier-Villars, Paris.

REOCREUX, M. 1974 Contribution a l'étude des debits critiques en écoulement diphasique eau–vapeur, Thèse, Univ. Scientifique et Médicale, Grenoble.

RIVKIN, S. L., ALEKSANDROV, A. A. & KREMENEVSKAYA, E. A. 1978 *Thermodynamic Derivatives for Water and Steam.* Winston, Washington, D.C.

SAHA, P., JO, J. H., NEYMOTIN, L., ROHATGI, U. S. & SLOVIK, G. 1982 Independent assessment of TRAC-PD2 and RELAP5/MOD1 codes at BNL in FY 1981. Report NUREG/CR-3148 BNL-NUREG-51645.

TRAPP, J. A. & RANSOM, V. H. 1982 A choked-flow calculation criterion for nonhomogeneous, nonequilibrium, two-phase flow. *Int. J. Multiphase Flow* **8**, 669–681.

APPENDIX A

Locus $\mathscr{S}$ as the Common Intersection of $\Delta = 0$ with all $N_i = 0$

Each of the conditions $N_i(z, \sigma^{**}) = 0$ defines a manifold Σ_i, which we assume to be n-dimensional. The set of singular points of [1] consists of the common intersection of the $n+1$ manifolds $\mathscr{T}, \Sigma_1, \ldots, \Sigma_n$. We now assert that, under the assumption of nondegeneracy, the set $\mathscr{S}$ lies at the intersection of just *two* manifolds, namely $\mathscr{T}(\Delta = 0)$ and *any one* of the manifolds Σ_i, say Σ_1. All other manifolds $\Sigma_i (i \neq 1)$ automatically intersect $\mathscr{T}$ *along* $\mathscr{S}$. This is equivalent to saying that substitution of the condition $\Delta = 0$ into the n conditions $N_i = 0$ results in a set of n linearly dependent equations.

The preceding assertions can be proved by recalling that in our case rank $A_{ij} = n - 1$, which means that of the n n-column vectors $(i = 1, \ldots, n)$,

$$\{A_{i1}, \ldots, A_{in}\} \text{ are linearly dependent} \qquad [A.1]$$

and

$$\{A_{i2}, \ldots, A_{in}\} \text{ are linearly independent.} \qquad [A.2]$$

The additional condition $N_1 = 0$ means that the n n-column vectors

$$\{b_i, A_{i2}, \ldots, A_{in}\} \text{ are also linearly dependent.} \qquad [A.3]$$

The linear dependence in [A.1]–[A.3] means that there exist numbers $\mu_2, \ldots, \mu_n$ and $\nu_2, \ldots, \nu_n$ with the property that

$$A_{i1}(\sigma^{**}) + \sum_{j=2}^{n} \mu_j A_{ij}(\sigma^{**}) = 0, \quad i = 1, \ldots, n, \qquad [A.4]$$

and

$$b_i(z^{**}, \sigma^{**}) + \sum_{j=2}^{n} \nu_j A_{ij}(\sigma^{**}) = 0, \quad i = 1, \ldots, n. \qquad [A.5]$$

Multiplying [A.4] by $\nu_\ell \neq 0$ and [A.5] by $\mu_\ell \neq 0$ and subtracting, we obtain the result that

$$\nu_\ell A_{i1}(\sigma^{**}) - \mu_\ell b_i(z^{**}, \sigma^{**}) + \sum_{j=2}^{n} (\mu_j \nu_\ell - \mu_\ell \nu_j) A_{ij}(\sigma^{**}) = 0. \qquad [A.6]$$

We note that the last term in [A.6] vanishes for $j = \ell$. This proves that the n-column vectors in which A_{ij} occurs in each column, with the exception of column ℓ which contains b_i, are linearly dependent. These linearly dependent vectors are of the form $\{A_{i1}, \ldots, A_{i,\ell-1}, b_i, A_{i,\ell+1}, \ldots, A_{in}\}$. Hence $N_1 = 0$ with $\Delta = 0$ implies that all $N_\ell = 0$, for $\ell = 2, \ldots, n$, on $\mathscr{S}$.

APPENDIX B

Transverse Intersection

We may assume that the set of $\mathscr{S}$ of nondegenerate singular points, being the intersection of two n-dimensional manifolds, will have the structure of an $(n-1)$-dimensional manifold. One may test the validity of this assumption in the vicinity of any fixed, nondegenerate singular point $(z^{**}, \boldsymbol{\sigma}^{**})$ by the following procedure. We compute the gradients of the functions $\Delta(\boldsymbol{\sigma})$ and $N_1(z, \boldsymbol{\sigma})$ at $(z^{**}, \boldsymbol{\sigma}^{**})$, viz.

$$\mathbf{h} = \begin{bmatrix} 0 \\ \hline \dfrac{\partial \Delta(\boldsymbol{\sigma}^{**})}{\partial \sigma_i} \end{bmatrix}, \qquad \mathbf{k} = \begin{bmatrix} \dfrac{\partial N_1(z^{**}, \boldsymbol{\sigma}^{**})}{\partial z} \\ \hline \dfrac{\partial N_1(z^{**}, \boldsymbol{\sigma}^{**})}{\partial \sigma_i} \end{bmatrix}. \tag{B.1}$$

When $\mathbf{h} \neq \mathbf{0}$, then $\mathscr{T}$ is, in the vicinity of $(z^{**}, \boldsymbol{\sigma}^{**})$, an n-dimensional surface which is normal to $\mathbf{h}$ at $(z^{**}, \boldsymbol{\sigma}^{**})$. Similarly, when $\mathbf{k} \neq \mathbf{0}$, then Σ_1 is, in the vicinity of $(z^{**}, \boldsymbol{\sigma}^{**})$, and n-dimensional surface which is normal to $\mathbf{k}$ at $(z^{**}, \boldsymbol{\sigma}^{**})$. If, further, $\mathbf{k}$ and $\mathbf{h}$ are linearly independent (i.e. noncollinear), then $\mathscr{T}$ and Σ_1 intersect transversely in the vicinity of $(z^{**}, \boldsymbol{\sigma}^{**})$ into a smooth $(n-1)$-dimensional manifold $\mathscr{S}$ on which $(z^{**}, \boldsymbol{\sigma}^{**})$ lies. The $(n-1)$-dimensional hyperplane tangent on $\mathscr{S}$ at $(z^{**}, \boldsymbol{\sigma}^{**})$ is the orthogonal complement of the two-dimensional subspace spanned by $\mathbf{h}$ and $\mathbf{k}$, i.e. a vector γ is tangent on $\mathscr{S}$ at $(z^{**}, \boldsymbol{\sigma}^{**})$ if and only if it is orthogonal to both $\mathbf{h}$ and $\mathbf{k}$ (figure B1).

APPENDIX C

Jacobian Matrix $e_{\alpha\beta}$

We propose to show that $n-1$ eigenvalues of the matrix $e_{\alpha\beta}$ must vanish. To this end we approach the singular point $(z^{**}, \boldsymbol{\sigma}^{**})$ along a curve given by the parametric equations $z = z(\tau)$, $\boldsymbol{\sigma} = \boldsymbol{\sigma}(\tau)$ and embedded in $\mathscr{S}$. Here τ is a parameter measured along curve $z(\tau)$ in $\mathscr{S}$, e.g. its arc

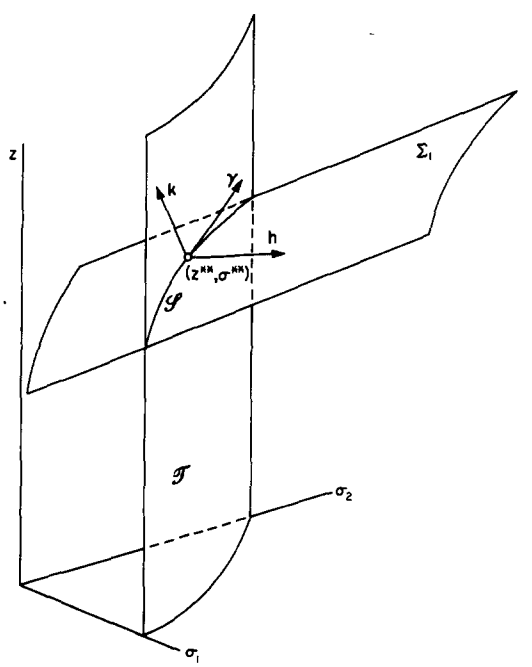

Figure B1. The vectors $\mathbf{h}$ and $\mathbf{k}$ in the phase space.

length. Since $\Delta = 0$ and $N_i = 0$ in $\mathscr{S}$, we note that

$$\Delta\{\boldsymbol{\sigma}(\tau)\} = 0, \quad N_i\{z(\tau), \boldsymbol{\sigma}(\tau)\} = 0, \quad i = 1, \ldots, n. \tag{C.1}$$

As $[z(0), \boldsymbol{\sigma}(0)] \equiv (z^{**}, \boldsymbol{\sigma}^{**})$, we can write the direction of an arbitrary vector γ tangential to the curve at the singular point by the components

$$\gamma = \{\dot{z}(0), \dot{\boldsymbol{\sigma}}(0)\}, \tag{C.2}$$

(the dot denotes $\partial/\partial\tau$). The formal derivatives of [C.1] give

$$0 = \dot{\Delta}(\tau) = \sum_{j=1}^{n} \frac{\partial \Delta(\boldsymbol{\sigma}^{**})}{\partial \sigma_j} \dot{\sigma}_j(0) = e_{\alpha\beta}\gamma_\beta \tag{C.3}$$

and

$$0 = N_i\{z(0), \boldsymbol{\sigma}(0)\} = \frac{\partial N_i(z^{**}, \boldsymbol{\sigma}^{**})}{\partial z} \dot{z}(0) + \sum_{j=1}^{n} \frac{N_i(z^{**}, \boldsymbol{\sigma}^{**})}{\partial \sigma_j} \dot{\sigma}_i(0) = e_{i\beta}\gamma_\beta, \quad i = 1, \ldots, n. \tag{C.4}$$

The preceding relations demonstrate that the directional derivatives $\dot{\Delta}(\tau)$ and $\dot{N}_i(\tau)$ appear in the form of the product of matrix $e_{\alpha\beta}$ and the tangent vector γ, i.e. in the form

$$e_{\alpha\beta}\gamma_\beta = 0, \quad \alpha = 0, 1, \ldots, n. \tag{C.5}$$

Since γ is an arbitrary vector lying in the $(n-1)$-dimensional manifold $\mathscr{S}$, it follows that zero is an eigenvalue of $e_{\alpha\beta}$ with multiplicity $n-1$. The matrix $e_{\alpha\beta}$ is a square $(n+1) \times (n+1)$ matrix and has, in addition, two other, presumably nonzero, eigenvalues $\lambda_1 \neq \lambda_2$.

APPENDIX D

Center Manifold Theorem

The "center manifold theorem" (Guckenheimer & Holmes 1983) states that the eigenspaces η, ξ of the linearized system $x_\alpha = e_{\alpha\beta}x_\beta$ corresponding to eigenvalues with nonzero real parts are tangent to trajectories of the full nonlinear system [1] at the singular point.